FEA-based multi-objective optimization of IPM motor design including rotor losses

(Article begins on next page)

17 May 2018

# FEA-based multi-objective optimization of IPM motor design including rotor losses

## G. Pellegrino
Member, IEEE
gianmario.pellegrino@polito.it
Politecnico di Torino
Corso Duca degli Abruzzi 24, Torino 10129, Italy

## F. Cupertino
Member, IEEE
cupertino@deemail.poliba.it
Politecnico di Bari
Via Orabona, 4, Bari 70125, Italy

*Abstract* – **The design optimization of IPM motors for wide speed ranges is considered in this paper by means of a FEA-based multi-objective genetic algorithm (MOGA). The minimum number of simulations is pursued for the fast evaluation of four goal functions: maximum torque, minimum torque ripple, maximum flux weakening capability and minimum rotor harmonic losses. The paper is focused on the rotor design, that is the most controversial aspect of IPM design due to the difficult modeling dominated by magnetic saturation. Three original results are presented: the elimination of higher order torque ripple harmonics and the minimization of FEA evaluations by means of a random rotor position offset and the evaluation, by means of the same static FEA runs, of the eddy current losses in the rotor core.**

*Index Terms -- Variable Speed Drives, Synchronous Motor Drives, Permanent magnet machines, Traction Motor Drives, Motor design optimization.*

## I. INTRODUCTION

Interior Permanent Magnet (IPM) motors are attractive for their flux weakening capability, associated with a good torque density and a high efficiency [1]. To obtain a large constant power speed range (CPSR), the IPM motor must be properly designed and the correct matching of permanent magnets (PM) flux and rotor magnetic saliency must be found [2]. The paper deals with the design of IPM motors with multi-layer rotor structures and inset magnets: such motors are characterized by a high magnetic saliency and a reduced quantity of PMs.

One key-issue in the design of such machines is to define the rotor geometry, that presents many degrees of freedom (number and shape of the layers, PM grade and placement). In the literature analytical [3] and lumped parameter models [4] are normally associated to FEA to account for magnetic saturation effects (saturation and cross-saturation) and all authors agree that saturation must be taken into account for a correct motor design [4,5]. Other key aspects are the minimization of the torque ripple [6] and of the high speed harmonic losses [7] that can be very high with poor design choices and are both difficult to be modeled by simple formulas. Optimization algorithms have been proposed for IPM motor design [8-10] but FEA-based optimization has been rarely adopted due to long computational time [10], except for the case of simpler rotor geometries with a single PM layer [15].

There is no general design approach based on FEA optimization, like the one proposed in [11] for surface mounted PM motors because on the one side the rotor geometry is more complicated and involves a higher number of parameters. From the other side, also the evaluation of the cost functions is more complicate here: the phase angle of the current is unknown a priori and the constant power speed range (CPSR), torque ripple and core losses require several FEA runs to be evaluated.

A first work has been presented with the aim of evaluating three cost functions (torque, torque ripple, CPSR) by a minimum set of FEA runs [16], and seven static simulations and about thirty seconds per tentative motor was the result at that time. In this work:

- the number of simulations per machine is reduced from seven to five with no loss of precision;
- the torque ripple minimization is improved by means of a randomly chosen rotor position offset;
- rotor losses are also evaluated as an additional cost function, with no extra FEA run.

Eddy current rotor losses, due to harmonic fields, have been included in the analysis because they limit the drive performance at high speed and must be minimized by proper design choices [7].

Two- and three-objective optimization results are presented for putting in evidence the relationships between input parameters and goal functions, between the different goal functions (some are in completion and some are not), and to draw general conclusions on rotor design optimization.
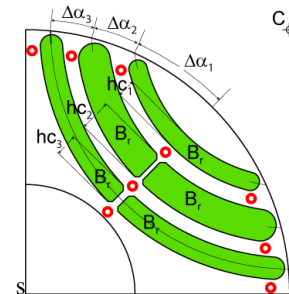


Figure 1. Example of rotor geometry with 3 layers: the $\Delta\alpha_j$ angles define the layer angular positions, $hc_j$ are the layer heights and $B_r$ defines the PM grade. The red circles stand for the point where the eddy-current loss is calculated.

## II. IPM MOTOR MODEL AND GOAL FUNCTIONS OF THE OPTIMIZATION

### A. Problem statement

The stator geometry is defined. The number of turns is preliminary chosen and can be adapted later for modifying the rated current and voltage of the optimal machine. The rated current $i_0$ is calculated according to the thermal load, expressed in stator Joule losses. The acceptable losses depend on the motor size and type of cooling. In case of overloaded machines, $i_0$ is the maximum inverter current. The rotor geometry parameters are defined in Fig. 1 for a 2 pole-pairs, 3 layers IPM motor. Bonded magnets that fill the layers completely are considered for simplicity. Nevertheless, the validity of the results can be easily extended to magnets of the sintered type. The rotor inter-layer ribs nearby the airgap are of a fixed width that depends on the bore diameter and on punching tolerance. The width of the radial ribs is calculated for withstanding a centrifugal stress of 180 N/mm$^2$ at overspeed. In case the calculated width is lower than the minimum accepted for punching, the rib is set to zero. The 3-layer rotor has been chosen as an example: machines with more layers can give a better performance, but they are also more difficult to be manufactured i.e. more expensive. Tthe number of layers is considered a preliminary choice of the designer, as a compromise between performance and construction cost. The size of the example motor is 3000W @ 5000rpm, 15000 rpm max speed; detailed ratings are reported in the section V.

### B. Simplified motor model

The simplified motor model (1) is introduced for pointing out the four cost functions: torque, torque ripple, CPSR, rotor losses.

$$\begin{cases} \lambda_d = \lambda_m + L_d \cdot i_d \\ \lambda_q = \xi \cdot L_d \cdot i_q \end{cases} \qquad (1)$$

$\lambda_m$ is the PM linked flux and $\xi = L_q/L_d$ is the saliency ratio [2]. The electromagnetic torque can be expressed as (2):

$$T = \frac{3}{2} p \cdot \left( \lambda_d \cdot i_q - \lambda_q \cdot i_d \right) =$$
$$= \frac{3}{2} p \cdot L_d \cdot i_0^2 \cdot \left( \frac{\lambda_m}{L_d i_0} \cdot \cos\gamma + \frac{\xi - 1}{2} \cdot \sin 2\gamma \right) \qquad (2)$$

where $p$ is the pole-pair number, $i_0$ is the current amplitude and $\gamma$ is the current phase angle. The two contributions called "PM torque" and "reluctance torque" are evidenced in (2).

### C. Maximum torque

According to (2), the maximum torque for a given current $i_0$ is obtained by a tradeoff between the PM torque and the reluctance torque. Magnetic saturation, that does not appear in (2), limits the machine rated flux and strongly determines the optimal tradeoff. Moreover, the rated current phase angle $\gamma_{MTPA}$, intended as the angle that gives the maximum torque

per Ampere (MTPA) for the given current $i_0$ is not known a priori and its evaluation would normally require several FEA runs for each tentative motor [10,15].

### D. Torque ripple

Torque ripple can be very high in IPM machines. For a given number of stator slots, the number of rotor layers and their position at the airgap ($\Delta\alpha_j$ angles defined in Fig. 1) are the factors that determine the torque ripple [6]. Rotor geometries leading to minimal ripple can be found either by moving the layer positions at the airgap or by choosing the correct rotor pitch with equally spaced layers. In this work, the number of layers is given, and their geometry is optimized by the algorithm.

### E. Constant power speed range

The flux weakening capability of an IPM motor drive depends of the matching of $\lambda_m$, $\xi$ and rated current $i_0$ [2]. In particular, the residual $d$-flux (3) will be minimized, that is the $d$-axis flux with the rated current aligned against the magnets. When (3) is zero the CPSR is virtually infinite.

$$\lambda_d\big|_{\gamma=90°} = \lambda_m - L_d \cdot i_0 \qquad (3)$$

The quantity (3) is easily evaluated with a single FEA run.

### F. Eddy current losses on the rotor

As for torque ripple, the rotor harmonic losses depend of the number of rotor layers, their position at the airgap and volume [7] and a trade-off must be found [12].

## III. MULTI-OBJECTIVE GENETIC OPTIMIZATION (MOGA)

The design of electric motors is a multi-objective problem i.e. the quest for a optimal compromise between many conflicting goals. Multi-objective optimization algorithms [13] search for a set of possible solutions according to the well known Pareto dominance criterion. Once the Pareto front is obtained the designer can select the preferred compromise among the different goals with a clear view of how much each objective is penalized by the improvement of another one. Thus the human decision comes after the automatic solution and not before, as it normally happens with single-objective optimization. It is very important that the functional evaluation, that is the evaluation of all the goal functions for each tentative solution, is computationally light in order to permit a high number of iterations in a reasonable time. Computation time is, up to date, the main limitation of FEA-based optimization.

### A. Evaluation of the different cost functions.

Dealing with **torque**, the knowledge of $\gamma_{MTPA}$ is needed for calculating the rated torque of the tentative motors. To avoid simulations for different trial values of $\gamma$, that would be time consuming, **the phase angle is included in the parameters to be optimized by the MOGA** and **each motor is evaluated for a single current angle that is selected by the MOGA**. It has

been demonstrated in [16] that for all the machines of the Pareto front the $\gamma_{MTPA}$ is correctly evaluated.

Dealing with **torque ripple**, *n* static simulations are run along one stator slot pitch and the standard deviation of the torque waveform is calculated. Due to the reduced number of evaluated positions, lower order ripple components can survive the optimization process but they are normally less critical. The minimum number of FEA runs *n* and its relationship with the elimination of higher order harmonics is addressed in section IV.

The **CPSR** is evaluated according to the minimization of (3). A single static simulation, in one rotor position, is run with $i_d = -i_0$ ($\gamma = 90°$). The optimal solutions are ranked in the Pareto front according to the residual *d* flux in this condition and the CPSR follows monotonically.

### B. Eddy current losses on the rotor

A dedicated subsection is spent for eddy current losses that are one of the contributions of the paper. The specific **eddy current losses** (W/m³) are calculated according to (4)

$$p_{eddy} = \frac{\sigma \cdot d^2}{12} \cdot \frac{\omega^2}{2\pi} \cdot \int_0^{2\pi} \left(\frac{\partial B}{\partial \vartheta}\right)^2 d\vartheta \qquad (4)$$

Where $\sigma$ is the electrical conductivity, *d* is the steel lamination thickness and steady-state electrical speed $\omega$ is assumed. The flux density $B(\theta)$ is evaluated in 3 points per each rotor yoke channel (see the red circles in Fig. 1) that means 9 points for a 3-layer rotor, and it is an output of the same *n* runs used for torque evaluation. No extra time is spent for evaluating $p_{eddy}$ because it is the post processing of already available FEA runs. The average of (4) over the three points of one yoke is multiplied for the volume of the respective yoke channel. All considered, the functional evaluation for calculating torque, torque ripple, CPSR and rotor losses of each tentative motor consists of *n*+1 static FEA runs, that less than 30 seconds computation time on a standard laptop computer (Intel Centrino T7200 @ 2 GHz) in case of *n* = 6.

TABLE I – ERROR IN THE CALCULATION OF TORQUE RIPPLE (STANDARD DEVIATION) FUNDAMENTAL COMPONENT AND 3RD HARMONIC WITH DIFFERENT NUMBERS OF SAMPLES *N*

| designator | | (a) | (b) | (c) |
|---|---|---|---|---|
| n | | 6 | 6 | 4 |
| $\Delta\theta_0$ | | 0 | Random | Random |
| $\Delta\theta_s$ | | $\tau_{st}/6$ | $\tau_{st}/6$ | $\tau_{st}/4.5$ |
| 1st harmonic | Average error | 10 % | 10 % | 20 % |
| | Maximum error | 10 % | 10 % | 25 % |
| 3rd harmonic | Average error | 100 % | 3 % | 11 % |
| | Maximum error | 100 % | 100 % | 20 % |

## IV. MINIMUM NUMBER OF FEA SIMULATIONS

The motor torque and losses are evaluated with *n* static FEA simulations in equally spaced rotor positions along one stator slot pitch ($\tau_{st}$). One slot pitch has been chosen because stator slots give the most significant torque ripple component in most of cases. Dealing with the torque ripple waveform, a certain number of simulations is required to avoid the aliasing of significant torque harmonics. For example, at least 3 points over one stator pitch are needed to capture the fundamental component of torque ripple. When 3rd harmonic is considered, 7 or more points are necessary. Higher order torque harmonics can also arise, but without a significant amplitude. Since the execution time of the MOGA practically coincides with the time devoted to the cost function evaluation (i.e. FEA simulations), the relationship between the number of FEA runs and the accuracy of the results is of key importance. As an example, if *n* = 6 (spacing between rotor position is $\tau_{st}/6$), the aliasing of the 3rd harmonic of the torque ripple will occur (see Fig. 2a). *To overcome this problem a random offset $\Delta\theta_0$ is superimposed to the simulated motor positions* (see Fig. 2b). The offset is randomly generated in the range $[0 \div \tau_{st}/6[$ for each tentative motor. As a side effect, the same motor, if evaluated twice, may be associated to different values of torque ripple. In other words, the random offset captures the 3rd harmonic ripple at the cost of making the functional evaluation noisy.
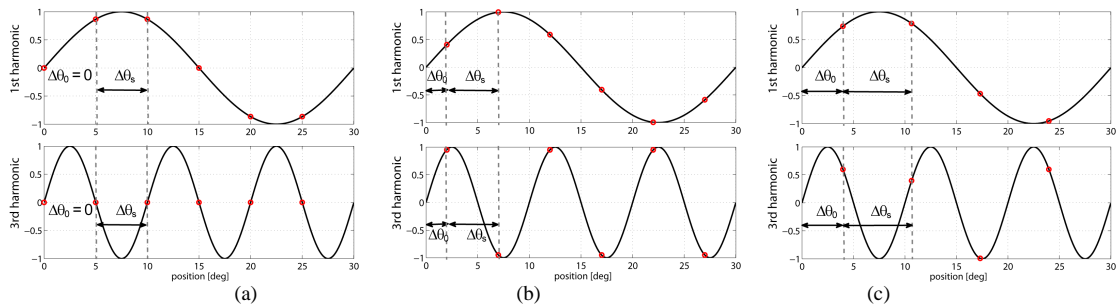


Figure 2. Fundamental and third harmonic of torque ripple regularly sampled using different sampling steps $\Delta\theta_s$ and offset $\Delta\theta_0$: (a) $\Delta\theta_s = \tau_{st}/6$, $\Delta\theta_0 = 0$; (b) $\Delta\theta_s = \tau_{st}/6$, $\Delta\theta_0$ = random; (c) $\Delta\theta_s = \tau_{st}/4.5$ and $\Delta\theta_0$ = random.

However, the stochastic nature of the MOGA filters the noise out of the cost function at the end of the optimisation process [14], resulting in the practical elimination of the 3rd harmonic with only 6 points instead of 7. Table I reports the average and maximum errors of the fundamental and 3rd harmonics of torque ripple calculated with different sampling techniques. The 3% average error on 3rd harmonic in line (b) confirms that the 3rd harmonic ripple can be evaluated and minimized by the MOGA. Such capability of the MOGA allows a further reduction of $n$. Fig 2c reports the fundamental and third harmonic sampled using only *four points and random offset*. With very few points the noise in the torque ripple evaluation increases. One heuristic approach to reduce such noise is to space the $n$ simulations by an angle that is not exactly $\tau_{st}/n$ as evidenced by the results reported in Table I for $\tau_{st}/(n+0.5)$. When the number of FEA simulations is lower than 4, the torque ripple evaluation becomes too coarse and the optimization algorithm converges to sub-optimal solutions.

## V. RESULTS OF THE OPTIMIZATION

First of all, the results of two different two-objective optimizations are presented, to put in evidence the effectiveness of the reduced number of FEA runs and the rate of competition between the different costs. In particular, torque and torque ripple are considered in the first subsection, as already done in [16], but with the minimized number of simulations (4 instead of 6, as said before). In subsection V.B a torque - rotor loss optimization is presented and the results are compared with the torque – ripple optimization.

Finally, two three-objective MOGA runs are shown, where the considered goals are: torque – ripple - CPSR and torque – ripple – rotor losses respectively.

For the two-objective runs and the last three-objective optimization the PM grade is set constantly to $B_r = 0.4$ T, while for the three-objective optimization that includes the CPSR in the goal functions, the $B_r$ is optimized by the MOGA. The ratings of the example motor are: 2 pole-pairs, 24 stator slots, current 14 Apk, voltage 280 V (pk, phase to phase), torque 5.7 Nm, rated speed 5000 rpm, max speed 15000 rpm, stack diameter – length 100 mm – 65 mm, natural air cooled.

### A. MOGA 2x: torque –ripple optimization (25 hours)

The results of torque-ripple optimisation are presented for the three different torque sampling modes introduced in Table I and Fig. 2. From each of the three Pareto fronts the solution with the minimum torque ripple has been chosen and the three solutions are compared in Fig. 3, indicated as (a), (b) and (c) according to Table I. The PM grade is set to $B_r = 0.4$ T for all the machines and all the MOGA runs, as will be better explained in the follwing. The torque waveforms of the three motors are also reported aside. It is evident from the figures that the 3rd harmonic ripple is not correctly eliminated by run (a), while it is minimized with the same effectiveness by runs

(b) and (c), thanks to the random offset $\Delta\theta_0$ addressed in section IV. Also the rotor geometries are the same for runs (b) and (c). Dealing with Fig. 3a, the blue circles indicate the six rotor positions evaluated by the optimization algorithm and clarify why the 3rd harmonic survived the optimization process without the adoption of the random offset. The results of Fig. 3 confirm that:

- the introduction of the random offset improves the torque ripple optimization leading to better rotor geometries.
- the correct geometry (Figs. 3b and 3c), with minimized ripple, can be obtained by simulating four positions instead of six, that is a reduction of the computational time by one third.

The Pareto front reported in Fig. 4 is the one of design (b) and puts in evidence that there is no competition between average torque and torque ripple, as also demonstrated in [16,17]: i.e. the machines with high and low ripple have nearly the same torque.
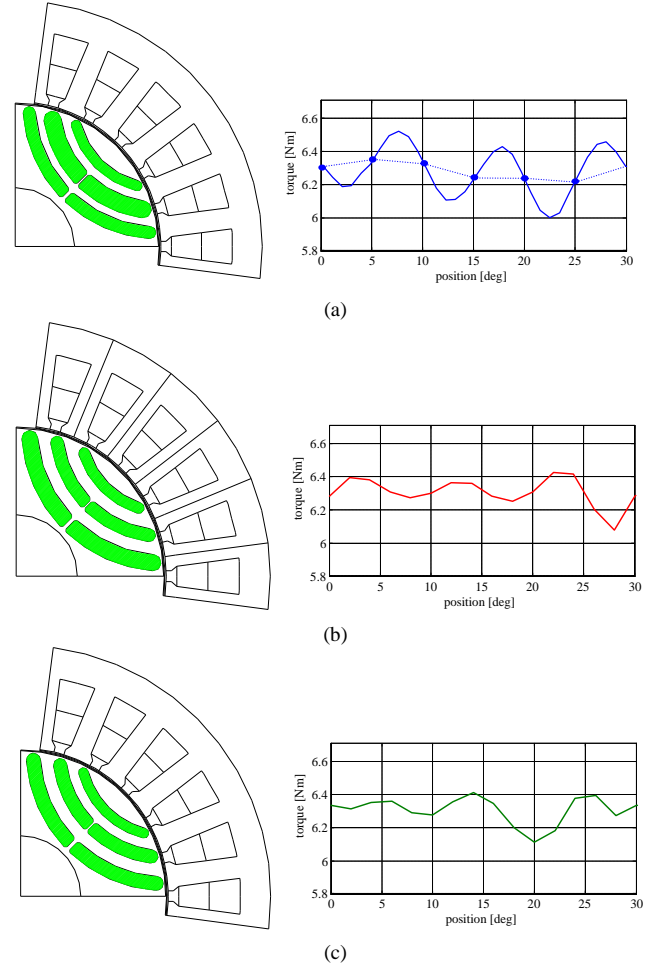


(a)



(b)



(c)

Figure 3. Rotor optimised with different number of FEM evaluations and related torque waveforms. a) 6 regularly distributed simulations ($\Delta\theta_s=\tau_{st}/6$) and no offest ($\Delta\theta_0=0$), b) 6 regularly distributed simulations ($\Delta\theta_s=\tau_{st}/6$) and random offset ($\Delta\theta_0$ = random); c) 4 simulations with reduced spacing ($\theta_s=\tau_{st}/4.5$) and random $\Delta\theta_0$.
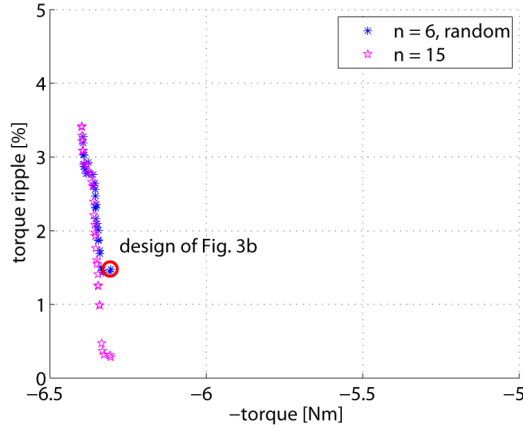
Figure 4. Pareto front of torque –ripple optimisation, type (b) of Table I (6 positions and random offset). Comparison between the output of the MOGA and the front recalculated with more detail (15 rotor position).

Moreover, the comparison of the Pareto front with the front obtained by re-calculating all the machines of the solution with more accuracy (15 rotor positions) confirms that random $n = 6$ leads to an accurate optimisation. As expected, the main difference between the two fronts of Fig. 4 is in the evaluation of the ripple, while the torque is correctly evaluated in both cases. The same comparison made for design (c) (with $n = 4$, 17 hours of computation) leads to more noisy results and has not been reported.

### B. MOGA 2x: torque –rotor loss optimization (25 hours)

The maximum torque – minimum loss optimization leads to the Pareto front of Fig. 5a. The losses are calculated at 1000rpm. The optimization has been run with $n = 6$ for the moment and with PM grade set to $B_r = 0.4$ T. As for Fig. 4, the Pareto front output by the MOGA, calculated with 6 random rotor positions, is re-calculated with 15 fixed rotor positions, that means calculated more accurately and the two fronts are compared in Fig. 5. The relationship between the two fronts is not so evident as in Fig. 4, since the Pareto front is replaced by a cloud of more sparse solutions. Four possible designs are presented (Fig. 6 a-d). From Figs. 5 and 6 it can be commented that:

- the two goal functions are in competition: low rotor losses can be achieved at the expense of a reduced rated torque;
- two branches can be distinguished in the Pareto front: a steep front on the left side, made of machines with high losses, that drop rapidly from one solution to the next at the expense of a limited torque reduction, and a flat front on the right side, where the losses are very small and the torque decreases rapidly. The optimal solution can be found at the corner of the two branches (Figs. 6a and 6b).
- For reducing the rotor loss, the MOGA tends to reduce the volume of the rotor iron, at the expense of an excessive torque reduction. It is clear that second rotor channel (from shaft to outside) is made thin by the MOGA (Figs. 6b and 6c) and this cuts most of the losses. Finally, also

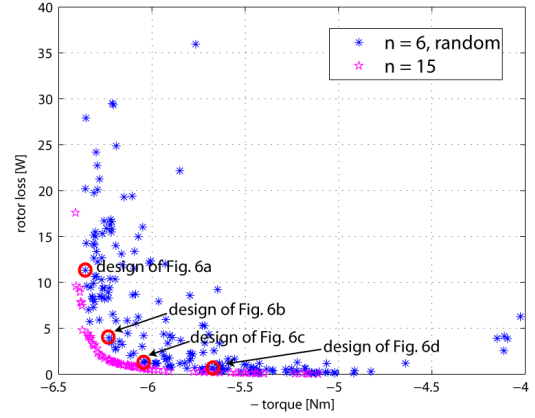the third rotor channel is minimized for further reducing the losses (Fig. 6d).



Figure 5. Pareto front of maximum torque – minimum rotor loss orptimisation run with 6 rotor positions and random offset (pink stars) and recalculated with 15 rotor positions (blue stars).
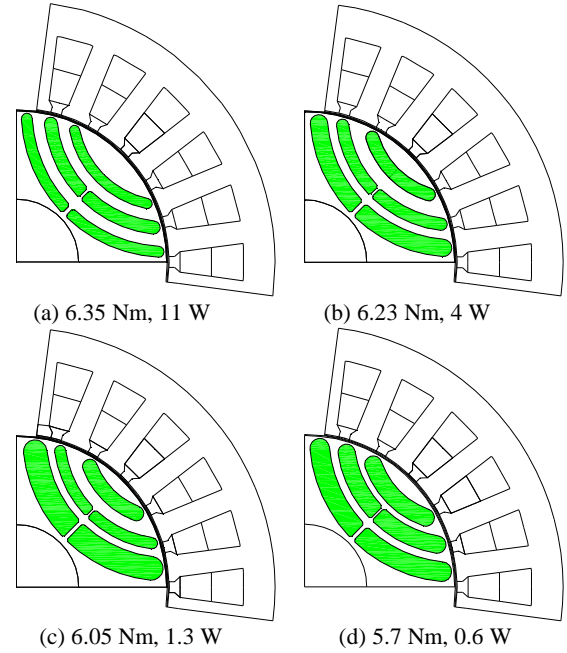


(a) 6.35 Nm, 11 W     (b) 6.23 Nm, 4 W

(c) 6.05 Nm, 1.3 W     (d) 5.7 Nm, 0.6 W

Figure 6. Designs selected from the Pareto front of Fig. 5. Below each figure the two goals are reported: torque and rotor loss.

### C. MOGA 3x: torque –ripple - CPSR (130 hours)

The torque –ripple –CPSR optimization leads to the Pareto front reported in Fig. 7. The three-objective optimization confirms that torque ripple is not in competition with the other goals: maximum torque (as said in V.A) and CPSR. On the contrary, torque and CPSR are in competition, as known from the literature [2]. In Fig. 8 the side view of Fig. 7 is reported, for putting in evidence the torque versus CPSR relationship and address the choice of the optimal machine. Apart for a group of solutions on the bottom of the front, where the CPSR is slightly augmented at the expense of a

significant torque reduction, the solution with the highest CPSR and low ripple is circled in red and represented in Fig. 10. From Fig. 8 it can be verified that the torque of a machine with infinite CPSR (6.2 Nm is the projection of the front on the *x*-axis) is 72% of the torque of a machine with no flux weakening capability (8.5 Nm, maximum torque solutions in Figs. 7 and 8). This confirms what is found in the literature, based on IPM machine models [2], where the expected ratio is 0.707.
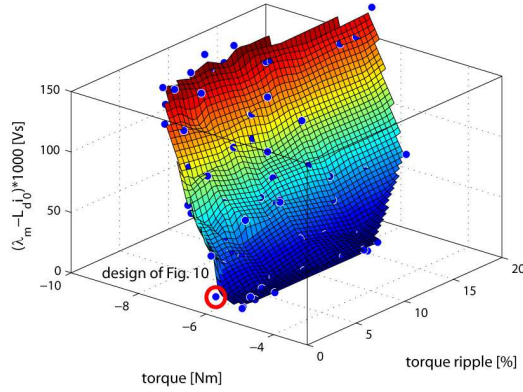


Figure 7. Pareto front of the torque-ripple-CPSR optimization. The CPSR is indicated (on the z-axis) by the residual *d*-axis flux (3).
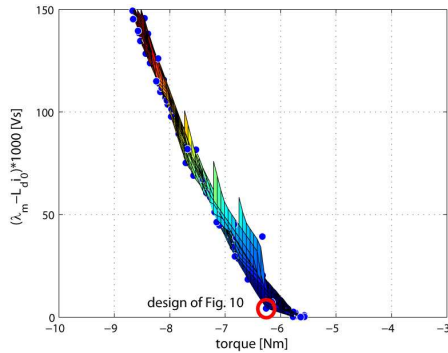


Figure 8. Side view of the Pareto front of Fig. 7 to put in evidence the relationship between torque and CPSR.
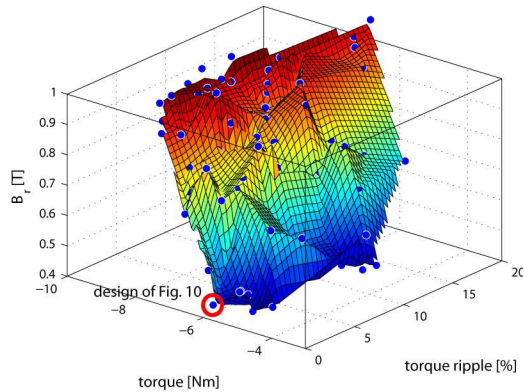


Figure 9. Front of the solutions of Fig. 7, where the PM grade $B_r$ is represented on the *z*-axis: apart for the scale factors, the two fronts of Figs. 7 and 9 are identical, showing the tight relationship between the PM grade and flux-weakening capability.
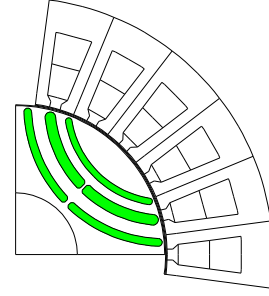


Figure 10. Best solution from the MOGA 3x (torque – ripple – CPSR), selected from the Pareto front of Fig. 7.

Last, the relationship between CPSR and PM grade is evidenced in Fig. 9, where the front of the solutions of Fig. 7 is reported with the PM grade $B_r$ along the *z*-axis instead of the residual *d*-flux. Apart for the scale factors, the two surfaces of Figs. 7 and 9 are very similar, that means that the CPSR almost exclusively depends of the PM grade. This also means that the CPSR of each solution can be varied and tuned by means of the choice of the PM grade, as also shown in [16]. For the motors under test the infinite CPSR condition coincides with $B_r = 0.4$ T, according to Fig. 9. For this reason the grade $B_r = 0.4$ T has been adopted throughout the paper, e.g. for two-dimensional optimizations of subsections V.A and B. It will be shown in the following that the machines presented in V.A and V.B have a large CPSR. The optimal machine of Fig. 10 has $B_r = 0.41$ T. In practical constructions the grades are standard but small variations have small effects on the CPSR.

### D. MOGA 3x: torque –ripple - rotor loss (110 hours)

The torque –ripple –rotor loss optimization leads to the Pareto front reported in Fig. 11 and Fig. 12 (side view). The torque to loss relationship is the same already found with MOGA2x (compare Fig. 12 with Fig. 5). On the other hand, the torque ripple to losses relationship seems to be non competitive, despite on this point is not definitely clarified in the literature, where design trade-offs are usually pursued [18].
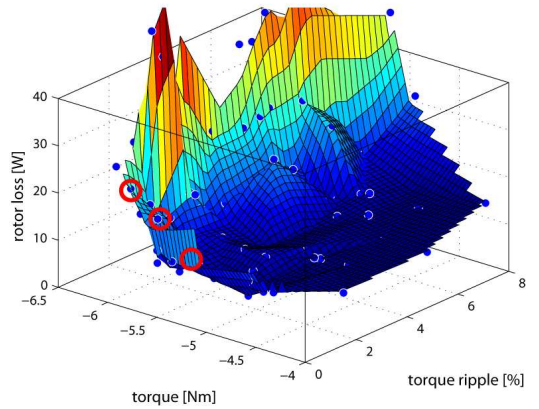


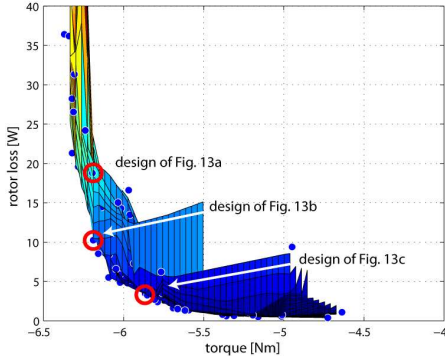Figure 11. Pareto front of the torque-ripple-rotor loss optimization.

Figure 12. Side view of the Pareto front of Fig. 11.



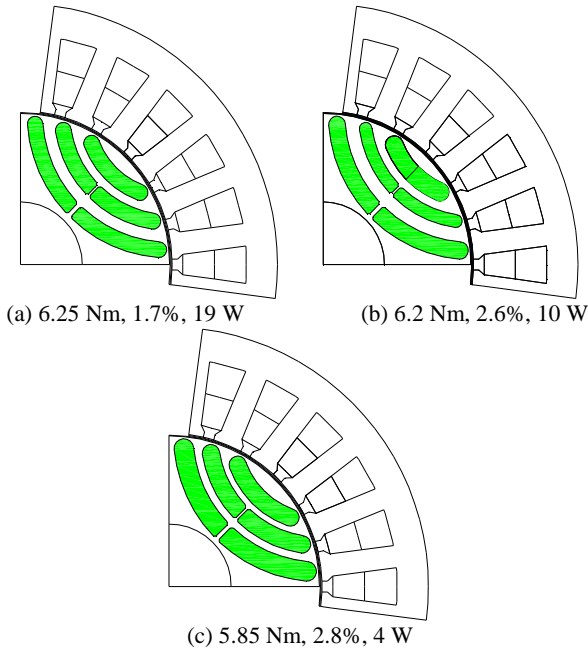(a) 6.25 Nm, 1.7%, 19 W  (b) 6.2 Nm, 2.6%, 10 W



(c) 5.85 Nm, 2.8%, 4 W

Figure 13. Designs selected from the Pareto front of Fig. 11. Below each figure the three goals are reported: torque, ripple (%) and rotor loss.

Three solutions are chosen with different torque to losses compromises and low ripple. They are reported in Fig. 13. As already noticed with torque – loss optimization (V.B), there is a part of the front where MOGA reduces the losses by reducing the volume of the iron channels, at the cost of a lower torque. The rotor iron reduction can be noticed progressively from Fig. 13a to 13c. Also in this case, the correct solution is found on the corner of the Pareto front, and the solutions of Fig. 13a and 13b are comparable and both valid: they have the same torque and a different combination of ripple and rotor losses.

### E.  Performance comparison of all the selected motors

The performance of all the considered solutions is evaluated and compared, in terms of the four goal functions considered in this paper. Namely, the torque waveforms at rated current, rated current angle and the power versus speed

curves at rated current will be reported for all the candidate motors. The value of rotor losses will be included in the labels referring to each motor.
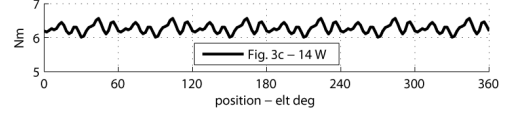


Figure 14. MOGA2x, torque – ripple. The torque waveform of Fig. 3c is reported here for the sake of comparison.
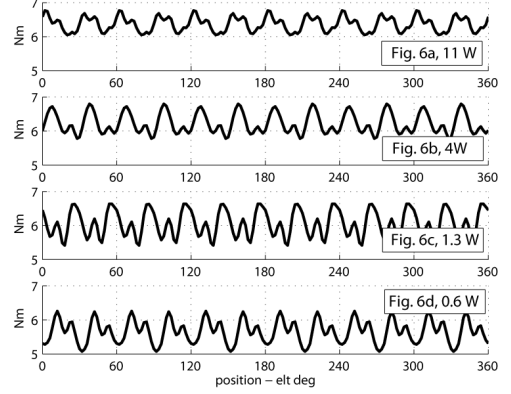


Figure 15. MOGA2x, torque – loss. The designs of Fig. 6, selected from the Pareto front of Fig. 5. Torque ripple is not optimized.
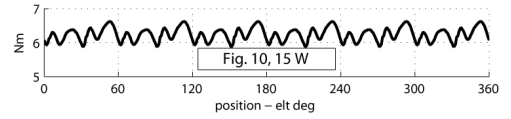


Figure 16. MOGA3x, torque – ripple - CPSR. The design of Fig. 10, selected from the Pareto front of Fig. 7.
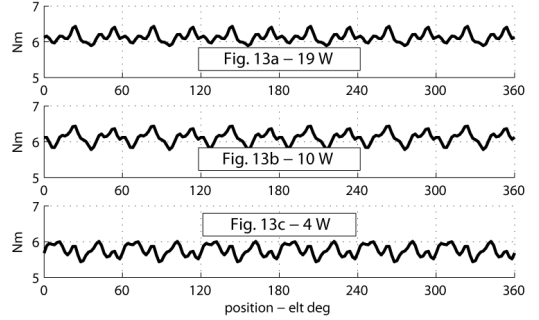


Figure 17. MOGA3x, torque – ripple –rotor loss. The designs of Fig. 6, selected from the Pareto front of Fig. 5.

### F.  General comments

All the proposed solutions have similar performances, in terms of torque and power curve at rated current, despite they are the outputs of different optimizations. This is mainly due to the choice of the proper PM grade $B_r = 0.4$ T, that result in a large CPSR and the same torque density for all the motors with this stator and this rated current. With a different stator or a different current load, the $B_r$ value for obtaining a high CPSR changes, but it can be easily evaluated without the necessity of a dedicated MOGA run.

When rotor losses are not minimized, they are still under

control (Fig. 14, Fig. 16), thanks to the ripple minimization, that leads to motors with a reduced content of harmonic fields. In a similar manner, when torque ripple is not minimized but the losses are, the ripple is significant but still under control, for the same reason (Fig. 15, Fig. 17).

For those motors where the rotor iron is reduced by the MOGA due to losses (Figs. 6d and 13c) the power profile, and the torque are significantly reduced.

All considered, the best tradeoff between computational time and performance, is given by MOGA2x, torque – ripple optimization, once the PM grade is known. As said, the correct PM grade can be found by running a first, quick MOGA2x with a trial $B_r$ value (e.g. $B_r = 0$ or any other value around 0.4T) and reduced population and generations size. Once selected a solution, $B_r$ can be adjusted for obtaining (3) equal to zero with a single FEA run or analytically. Finally, a complete MOGA2x can be run.
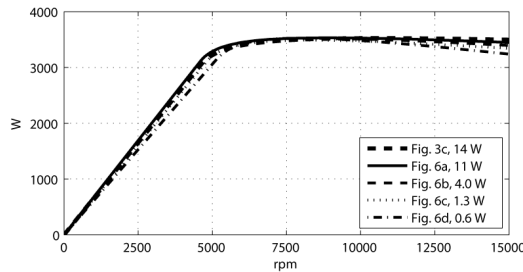


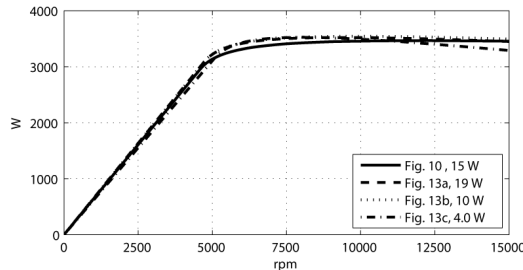Figure 18. Summary of all the MOGA2x solutions. Power profiles of the designs of Figs. 3c and 6, at rated current $i_0$.



Figure 19. Summary of all the MOGA3x solutions. Power profiles of the designs of Figs. 10 and 13, at rated current $i_0$.

## VI. CONCLUSIONS

The design optimization of a IPM motor rotor with three layers has been proposed, based on a multi-objective genetic algorithm and static FEA runs. Three original results have been presented: minimal numbers of FEA runs (4 to 7) for evaluating up to four goal functions, the introduction of a position offset that minimizes the torque ripple contributing to a reduced number of simulations and the evaluation of rotor core high speed losses. A series of results is presented, and conclusions are drawn for addressing the best compromise between computational time and performance of the solutions.

REFERENCES

[1] R. Schiferl,T.A. Lipo, "Power capability of Salient pole P.M. synchronous motors in variable speed drive", *Conf. Record. of IEEE-IAS annual meeting 1988*, pp: 23-31.

[2] W. Soong and T. J. E. Miller, "Field weakening performance of brushless synchronousAC motor drives," *Proc. IEE—Elect. Power Appl.*, vol. 141, no. 6, pp. 331–340, Nov. 1994.

[3] A. Fratta, A. Vagati, F. Villata, "Design criteria of an IPM machine suitable for field-weakening operation", *International Conference on Electrical Machines*, ICEM90, Boston 1990, U.S.A., pp: 1059-1065.

[4] Lovelace, E.C.; Jahns, T.M.; Lang, J.H., "Impact of saturation and inverter cost on interior PM synchronous machine drive optimization," *Industry Applications, IEEE Transactions on* , vol.36, no.3, pp.723-729, May/Jun 2000.

[5] N. Bianchi, S. Bolognani, A. Consoli, T.M. Jahns, R.D. Lorenz, E.C. Lovelace, S. Morimoto, A. Vagati, "Design, analysis, and control of interior PM synchronous machines," *in Proc. IEEE IAS Tutorial Course Notes, IAS Annu. Meeting*, N. Bianchi and T. M. Jahns, Eds. Seattle, WA: CLEUP, Oct. 3, 2004.

[6] Jahns, T.M.; Soong, W.L., "Torque Ripple Reduction in Interior Permanent Magnet Synchronous Machines Using the Principle of Mutual Harmonics Exclusion," *Industry Applications Conference, 2007. 42nd IAS Annual Meeting. Conference Record of the 2007 IEEE* , vol., no., pp.558-565, 23-27 Sept. 2007

[7] Han, S.-H.; Jahns, T. M.; Zhu, Z. Q., "Analysis of Rotor Core Eddy-Current Losses in Interior Permanent-Magnet Synchronous Machines," *Industry Applications, IEEE Transactions on* , vol.46, no.1, pp.196-205, Jan.-feb. 2010

[8] Sibande, S.E.; Kamper, M.J.; Wang, R.; Rakgati, E.T., "Optimal design of a PM-assisted rotor of a 110 kW reluctance synchronous machine," *AFRICON, 2004. 7th AFRICON Conference in Africa* , vol.2, no., pp. 793-797 Vol.2, 15-17 Sept. 2004

[9] Raminosoa, T.; Rasoanarivo, I.; Sargos, F.-M.; Andriamalala, R.N., "Constrained Optimization of High Power Synchronous Reluctance Motor Using Non Linear Reluctance Network Modeling," *Industry Applications Conference, 2006. 41st IAS Annual Meeting. Conference Record of the 2006 IEEE* , vol.3, no., pp.1201-1208, 8-12 Oct. 2006

[10] Wen Ouyang; Zarko, D.; Lipo, T.A., "Permanent Magnet Machine Design Practice and Optimization," *Industry Applications Conference, 2006. 41st IAS Annual Meeting. Conference Record of the 2006 IEEE* , vol.4, no., pp.1905-1911, 8-12 Oct. 2006

[11] Bianchi, N.; Bolognani, S., "Design optimisation of electric motors by genetic algorithms," *Electric Power Applications, IEE Proceedings -* , vol.145, no.5, pp.475-483, Sep 1998.

[12] Han, S.-H.; Jahns, T. M.; Zhu, Z. Q., "Design Tradeoffs Between Stator Core Loss and Torque Ripple in IPM Machines," *Industry Applications, IEEE Transactions on* , vol.46, no.1, pp.187-195, Jan.-feb. 2010

[13] K. Deb, "Multi-objective optimization using evolutionary algorithms", *Wiley-Interscience Series in Systems and Optimization*, 2001.

[14] K. Deb, A. Patrap, S. Agarwal, and T. Meyarivan: "A Fast and Elitist Multiobjective Genetic Algorithm: NSGA-II", *IEEE Transactions on Evolutionary Computation*, vol. 6, n. 2, April 2002, pp. 182-197.

[15] Bianchi, N.; Canova, A.; , "FEM analysis and optimisation design of an IPM synchronous motor," *Power Electronics, Machines and Drives, 2002. International Conference on (Conf. Publ. No. 487)* , vol., no., pp. 49- 54, 4-7 June 2002

[16] G. Pellegrino and F. Cupertino, "IPM motor rotor design by means of FEA-based multi-objective optimization", *IEEE International Symposium on Industrial Electronics*, ISIE 2010, Bari 4-7 July 2010.

[17] P. Alotto, M. Barcaro, N. Bianchi and M. Guarnieri, "Optimization of Interior PM Motors with Machaon Rotor Flux Barriers", CEFC 2010.

[18] G. Pellegrino, P. Guglielmi, A. Vagati and F. Villata, "Core loss and torque ripple in IPM machines: dedicated modeling and design trade off", *Energy Conversion Congress and Exposition*, ECCE 2009, San Jose, California, 20-24 September 2009, p. 1911-1918.